UCRL-JRNL-223245

The Heavy-Ion Approximation for Ambipolar Diffusion Calcuations for Weakly Ionized Plasmas

P. Li, C. McKee, R. Klein

July 28, 2006

Astrophysical Journal

The Heavy-Ion Approximation for Ambipolar Diffusion Calculations for Weakly Ionized Plasmas

Pak-Shing Li

Astronomy Department, University of California, Berkeley, CA 94720

psli@astron.berkeley.edu

Christopher F. McKee

Physics Department and Astronomy Department, University of California, Berkeley, CA 94720

cmckee@astro.berkeley.edu

and

Richard I. Klein

Astronomy Department, University of California, Berkeley, CA 94720; and Lawrence Livermore National Laboratory,
P.O.Box 808, L-23, Livermore, CA 94550

klein@astron.berkeley.edu

ABSTRACT

Ambipolar diffusion redistributes magnetic flux in weakly ionized plasmas and plays a critical role in star formation. Simulations of ambipolar diffusion using explicit MHD codes are prohibitively expensive for the level of ionization observed in molecular clouds ($\lesssim 10^{-6}$) since an enormous number of time steps is required to represent the dynamics of the dominant neutral component with a time step determined by the trace ion component. Here we show that ambipolar diffusion calculations can be significantly accelerated by the "heavy-ion approximation," in which the mass density of the ions is increased and the collisional coupling constant with the neutrals decreased such that the product remains constant. In this approximation, the ambipolar diffusion time and the ambipolar magnetic Reynolds number remain unchanged. We present three tests of the heavy-ion approximation: C-type shocks, the Wardle instability, and the 1D collapse of a magnetized slab. We show that this approximation is quite accurate provided that (1) the square of the Alfvén Mach number is small compared to the ambipolar diffusion Reynolds number for dynamical problems, and that (2) the ion mass density is negligible for quasi-static problems; a specific criterion is given for the magnetized slab problem. The first condition can be very stringent for turbulent flows with large density fluctuations.

Subject headings: Magnetic fields—MHD—ISM: magnetic fields—ISM: kinematics and dynamics—stars:formation

1. Introduction

Astrophysical plasmas generally have both neutral and ionized components, which are coupled by ion-neutral collisions. Magnetic stresses are directly coupled to the ions, and can be communicated to the neutrals only through these collisions. If the ions are well-coupled to the magnetic field (i.e., the gyrofrequency is large compared to the collision frequency), then the ions and magnetic field can move with respect to the neutrals in a process termed ambipolar diffusion (Mestel & Spitzer 1956). Ambipolar diffusion is particularly important in star formation, where it is believed to be the dominant mechanism responsible for resolving the magnetic flux problem, which is that the flux-to-mass ratio in the interstellar medium is orders of magnitude greater than that in stars (Mestel & Spitzer 1956; Mestel 1985; Mouschovias 1987). Indeed, if the magnetic field strength is large enough that the mass-to-flux ratio is less than a critical value (i.e., the cloud is "magnetically subcritical"), the cloud cannot collapse gravitationally in the absence of ambipolar diffusion (Mestel & Spitzer 1956). Subsequent studies of star formation with subcritical initial conditions by Mouschovias and his collaborators and others (Mouschovias 1976a,b; Shu 1983; Shu, Adams, & Lizano 1987; McKee 1989; Fiedler & Mouschovias 1993; Basu & Mouschovias 1994) concluded that ambipolar diffusion driven core collapse can explain the time scale of star formation, which is the result of the ambipolar diffusion time scale; the very low mass-to-flux ratio observed in new born stars, which is the result of re-distribution of magnetic field due to ambipolar diffusion; and the low angular momentum of new born stars because of magnetic braking. Turbulent motions can accelerate ambipolar diffusion by creating strong gradients in the field (Zweibel 2002; Fatuzzo & Adams 2002). Although observations have shown that cores are generally magnetically critical rather than subcritical (Crutcher 2005), ambipolar diffusion remains an essential process in the formation of stars. Ambipolar diffusion is also of critical importance in shock waves in weakly ionized plasmas (Draine 1980; Chernoff 1987; Draine & McKee 1993). For shock velocities less than ~ 50 km s^{-1} (Draine & McKee 1993) and ionizations low enough that the ion Alfvén velocity $v_{Ai} \equiv B/(4\pi\rho_i)^{1/2}$ considerably exceeds the shock velocity v_s, the ions and magnetic field can smoothly decelerate the neutrals such that there is no jump in the density and temperature of the neutrals on the scale of the neutral mean free path. Such shocks are termed "C-shocks" (Draine 1980) and are the dominant form of shock in weakly ionized molecular gas. Because of the complexities involved in magneto-hydrodynamic (MHD) turbulence and in the gravitational collapse of magnetized molecular clouds, numerical simulation is essential for studying these processes. With advances in massively parallel supercomputing platforms, highly parallelized, explicit MHD codes, such as ZEUS-MP (Norman 2000), are widely used in these investigations (e.g. Li et al. 2004). The use of ZEUS-MP is restricted to ideal MHD, however. When ambipolar diffusion is considered, the time step in explicit schemes is restricted $\Delta t \propto \Delta x^2/v_A v_{Ai} \propto \chi_i^{1/2}$, where $\chi_i \equiv \rho_i/\rho$ is the ionization mass fraction. In molecular clouds, the ionization can be low enough that $v_{Ai} \gtrsim 10^3$ km s^{-1}, making

$\Delta t \sim 10^3$ times smaller than in an ideal MHD calculation. Equivalently, the ion-neutral drag term in the momentum equation makes the equation very stiff for low ionization. Mac Low & Smith (1997) developed a semi-implicit scheme to update the coupled momentum equations for ions and neutrals such that $\Delta t \lesssim \Delta x/v_{Ai}$, but this remains proportional to $\chi_i^{1/2}$. For molecular cloud cores, which can have ionization fractions $\lesssim 10^{-7}$ (e.g. Caselli et al. 1998; Bergin et al. 1999), it is totally impractical to perform 3-dimensional (3-D) simulations of ambipolar diffusion driven core collapse using explicit MHD codes. Some semi-implicit or fully implicit 2-D schemes have been proposed to handle multifluid magnetohydrodynamics with stiff terms (e.g. Fiedler & Mouschovias 1992; Tóth 1995; Hujeirat & Rannacher 2001; Falle 2003; O′Sullivan & Downes 2005). The timestep may be greatly improved using these schemes, but at the expense of a substantial increase in complexity for 3-D codes. A fully implicit method requires matrix solutions and many iterations to converge to the solution at each step and may not significantly reduce the computation time. In this paper, we investigate a simple method to accelerate explicit 2-fluid MHD simulations with ambipolar diffusion. In the next section, we summarize the equations we solve, describe the numerical method, and discuss the simple method to speed up ambipolar diffusion calculation. In §3, we present three test problems to demonstrate the method and the criterion for using the method: the structure of a C-shock, the Wardle instability (Wardle 1990), and a variant of the slab ambipolar diffusion problem considered by Shu (1983). We summarize our findings in §4.

2. Methodology

2.1. Basic Equations

We assume that the ions are well-coupled to the magnetic field ($\omega_{ci}\tau_{\mathrm{coll},\,i} \gg 1$, where ω_{ci} is the ion gyrofrequency and $\tau_{\mathrm{coll},\,i}$ is the ion collisional time); it follows that the relative velocity between the electrons and the ions is negligible. In our work, we also assume that there is no recombination or ionization, so that the number of charged particles is conserved. Let ρ be the mass density, $\mathbf{v}$ the velocity, P the pressure, $\mathbf{B}$ the magnetic field strength, $\mathbf{g}$ the gravitational acceleration, and γ the ion-neutral collisional coupling constant, and let the subscript i denote ions and n neutrals. The 2-fluid equations of MHD are then (Shu 1992)

$$\frac{\partial \rho_n}{\partial t} = -\nabla \cdot (\rho_n \mathbf{v}_n), \tag{1}$$

$$\frac{\partial \rho_i}{\partial t} = -\nabla \cdot (\rho_i \mathbf{v}_i), \tag{2}$$

$$\rho_n \frac{\partial \mathbf{v}_n}{\partial t} = -\rho_n(\mathbf{v}_n \cdot \nabla)\mathbf{v}_n - \nabla P_n - \gamma \rho_i \rho_n (\mathbf{v}_n - \mathbf{v}_i) + \rho_n \mathbf{g}, \tag{3}$$

$$\rho_i \frac{\partial \mathbf{v}_i}{\partial t} = -\rho_i(\mathbf{v}_i \cdot \nabla)\mathbf{v}_i - \nabla P_i - \gamma \rho_i \rho_n (\mathbf{v}_i - \mathbf{v}_n) + \rho_i \mathbf{g} + \frac{1}{4\pi}(\nabla \times \mathbf{B}) \times \mathbf{B}, \tag{4}$$

$$\frac{\partial \mathbf{B}}{\partial t} = \nabla \times (\mathbf{v}_i \times \mathbf{B}), \tag{5}$$

$$\nabla \cdot \mathbf{B} = 0, \tag{6}$$

plus the energy equation. We assume that the system is isothermal, $P_{i,\,n} = \rho_{i,\,n} c_s^2$, so that the energy equation is not needed. The ion-neutral drag coefficient is (see Draine, Roberge & Dalgarno 1983)

$$\gamma = \frac{\langle w\sigma_{in}\rangle}{(m_n + m_i)} = \gamma_0 \, \mathrm{Max}\left(1, \frac{|\mathbf{v}_i - \mathbf{v}_n|}{v_\gamma}\right), \tag{7}$$

where σ_{in} is the ion-neutral cross section, m_n is the average mass of a neutral particle, m_i the average mass of an ion,

$$\gamma_0 = \frac{1.9 \times 10^{-9}}{(m_n + m_i)} \ \ \mathrm{cm}^3 \ \mathrm{s}^{-1}, \tag{8}$$

and $v_\gamma = 19$ km s^{-1} is the value of the drift velocity at which the Langevin approximation $\langle w\sigma_{in}\rangle = $ const breaks down. In a molecular gas with 10% He by number, the mean neutral mass is $m_n = 2.33 m_{\rm H}$. Observationally, the mean ion mass can vary from $30 m_{\rm H}$ to $3 m_{\rm H}$, depending on the fractional abundances of heavy ions such as HCO^+ and light ions such as H_3^+ (Caselli et al. 2002). The ionization is generally described in terms of the ratio of the number density of ions to that of hydrogen nuclei, $x_i \equiv n_i/n_{\rm H}$. However, the dynamics are governed by the ratio of the mass densities,

$$\chi_i \equiv \frac{\rho_i}{\rho} = \frac{x_i m_i}{\mu_{\rm H}}, \tag{9}$$

where $\mu_{\rm H}$ is the mean mass per hydrogen nucleus; for 10% He by number, $\mu_{\rm H} \equiv \rho/n_{\rm H} = 1.4 m_{\rm H} = 2.34 \times 10^{-24}$ g. For example, if $m_i = 10 m_{\rm H}$, then $\chi_i = 7.1 x_i$.

2.2. Inertial Forces and Ambipolar Diffusion

We can rewrite the ion equation of motion schematically as

$$\mathbf{f}_I + \mathbf{f}_D + \mathbf{f}_L = 0, \tag{10}$$

where

$$\mathbf{f}_I \equiv \rho_i \left(-\frac{d\mathbf{v}_i}{dt} - \frac{1}{\rho_i}\nabla P_i + \mathbf{g}\right) \tag{11}$$

is the ion inertial force (proportional to the ion density), $\mathbf{f}_D = -\gamma\rho_i\rho_n(\mathbf{v}_i - \mathbf{v}_n)$ is the drag force on the ions, and $\mathbf{f}_L$ is the Lorentz force. Observe that when the Lorentz force dominates the inertial force, the drag force $\mathbf{f}_D \simeq -\mathbf{f}_L$ becomes independent of ρ_i. Solving equation (10) for the ion velocity yields

$$\mathbf{v}_i = \mathbf{v}_n + \frac{1}{\gamma\rho_i\rho_n}\left(\mathbf{f}_L + \mathbf{f}_I\right). \tag{12}$$

The induction equation (5) then becomes

$$\frac{\partial \mathbf{B}}{\partial t} + \nabla\times(\mathbf{B}\times\mathbf{v}_n) = -\nabla\times\left[\frac{\mathbf{B}\times(\mathbf{f}_L + \mathbf{f}_I)}{\gamma\rho_i\rho_n}\right], \tag{13}$$

$$= \nabla\times\left\{\frac{\mathbf{B}\times[\mathbf{B}\times(\nabla\times\mathbf{B}) - 4\pi\mathbf{f}_I]}{4\pi\gamma\rho_i\rho_n}\right\}. \tag{14}$$

The case in which the Lorentz force dominates the inertial force, so that $\mathbf{f}_I$ can be neglected in the induction equation, corresponds to classical ambipolar diffusion. The characteristic value of the Lorentz force is $f_L \sim B^2/4\pi\ell_B$, where $\ell_B \equiv |B/\nabla B|$. The corresponding characteristic drift velocity between the ions and the neutrals is (eq. 12 with $\mathbf{f}_I = 0$):

$$v_{\rm AD} \equiv \frac{B^2}{4\pi\gamma\rho_i\rho_n\ell_B}. \tag{15}$$

The corresponding ambipolar diffusion timescale is

$$t_{\rm AD} \equiv \frac{\ell_B}{v_{\rm AD}} = \frac{4\pi\gamma\rho_i\rho_n\ell_B^2}{B^2} = \frac{\ell_B^2}{t_{ni}v_A^2}, \tag{16}$$

where $t_{ni} \equiv 1/(\gamma\rho_i)$ is the ion-neutral collision time. The length scale for ambipolar diffusion is the value of ℓ_B for which the ambipolar diffusion velocity equals the flow velocity v,

$$\ell_{\rm AD} \equiv \frac{B^2}{4\pi\gamma\rho_i\rho_n v}. \tag{17}$$

The magnetic Reynolds number for ambipolar diffusion over a length scale ℓ is (Zweibel 2002)

$$R_{\rm AD}(\ell) \equiv \frac{\ell v}{t_{ni}v_A^2} = \frac{4\pi\gamma\rho_i\rho_n\ell v}{B^2} = \frac{\ell}{\ell_{\rm AD}}; \tag{18}$$

ambipolar diffusion is negligible on a scale ℓ if $\ell \gg \ell_{\rm AD}$, or $R_{\rm AD}(\ell) \gg 1$.

Ambipolar diffusion introduces characteristic length scales for the propagation of Alfvén waves (Kulsrud & Pearce 1969). At sufficiently low frequencies, Alfvén waves propagate in the coupled ion-neutral fluid with a dispersion relation $\omega = k_\parallel v_A$, where $k_\parallel$ is the component of $\mathbf{k}$ parallel to $\mathbf{B}_0$. As the wavenumber increases, damping becomes increasingly important, and the waves cease propagating at all for wavenumbers $k_\parallel$ greater than

$$k_{\rm low} \equiv \frac{2}{v_A t_{ni}}. \tag{19}$$

On the other hand, above a wavenumber

$$k_{\rm high} \equiv \frac{1}{2\chi_i^{1/2} v_A t_{ni}} \tag{20}$$

waves can propagate in the ion fluid with $\omega \simeq k_\parallel v_{Ai}$. (These results apply to fast magnetosonic waves propagating perpendicular to the field if $k_\parallel$ is replaced by k.) Since $k_{\rm high}/k_{\rm low} = 1/(4\chi_i^{1/2})$, there is a range of wavenumbers, $k_{\rm low} < k < k_{\rm high}$, in which no Alfvén waves can propagate provided $4\chi_i^{1/2} < 1$, or $\chi_i < 1/16$.

These results for wave propagation can be understood in terms of the discussion of the ambipolar diffusion timescale, $t_{\rm AD}$, if we alter the definition of ℓ_B so that it applies to waves with small amplitudes, $\delta B \ll B$. We define $\ell_{\delta B} = |\delta B/\nabla\delta B|$, so that $\ell_{\delta B} = k^{-1}$. For this heuristic discussion,

we shall assume that the Alfvén waves propagate along the magnetic field, so that $k_\parallel = k$ (as remarked above, the discussion also applies to fast magnetosonic waves propagating normal to the field). For the low-frequency waves to propagate, we require

$$\omega t_{\rm AD}(\ell_{\delta B}) \simeq k v_A \cdot \frac{1}{k^2 t_{ni} v_A^2} > 1 \tag{21}$$

so that the ambipolar diffusion time is longer than the wave period; this implies $k < \frac{1}{2} k_{\rm low}$, close to the exact result. For high frequencies, the ambipolar diffusion time must be so short that the ions are decoupled from the neutrals:

$$\omega t_{\rm AD}(\ell_{\delta B}) \simeq k v_{Ai} \cdot \frac{1}{k^2 t_{ni} v_A^2} < 1. \tag{22}$$

This implies $k > 2k_{\rm high}$, which again is close to the exact result.

As noted above, the ion inertial force is generally neglected in treatments of ambipolar diffusion, which is valid provided the inertial force is small compared to the drag force. We write the inertial force as

$$f_I = \frac{\rho_i v_i^2}{\ell_{v_i}}, \tag{23}$$

where ℓ_{v_i} is the length scale over which the ion velocity changes, $\ell_{v_i} \sim |v_i/\nabla v_i|$. The condition $f_I \ll f_D$ implies

$$\frac{\rho_i v_i^2}{\ell_{v_i}} \ll \gamma \rho_i \rho_n |v_i - v_n| \lesssim \gamma \rho_i \rho_n v, \tag{24}$$

$$\Rightarrow \quad \mathcal{M}_{Ai}^2 \ll R_{\rm AD}(\ell_{v_i}). \tag{25}$$

Equation (25) gives the criterion for neglecting the ion inertia in smooth flows. In turbulent flows, $\mathcal{M}_{Ai}^2$ and $R_{\rm AD}$ can have large fluctuations. As a result, care must be exercised in using the heavy-ion approximation for turbulent flows. Note that $R_{\rm AD}(\ell_{v_i}) \propto \ell_{v_i}$; for small oscillations, we expect $\ell_{v_i} \sim \ell_{\delta B} \sim k^{-1}$, whereas if the field is strongly distorted by the flow ($\delta B \sim B$), we expect $\ell_{v_i} \sim \ell_B$.

We see that deviations from ideal MHD, in which $v_i = v_n$, are governed by two parameters: $\mathcal{M}_{Ai}^2$, which describes the importance of inertial forces, and the magnetic Reynolds number for ambipolar diffusion, $R_{\rm AD}(\ell_{v_i})$. In simple flows, there is a well-defined value of ℓ_{v_i} and ambipolar diffusion can be described by a single characteristic value, but in turbulent flows one needs the functions $\mathcal{M}_{Ai}^2(\ell)$ and $R_{\rm AD}(\ell)$. Provided the electrons are tightly coupled to the ions (i.e., Hall currents are negligible), as we have assumed, non-ideal MHD must be addressed with the two-fluid equations given at the beginning of this section. However, if the ion inertia is negligible, these equations reduce to single-fluid equations, with the Lorentz force replacing the drag force in the equation of motion for the neutrals. In our numerical work in this paper, we shall use the full two-fluid equations.

2.3. Dimensionless Parameters

It is often convenient to express the equations in dimensionless form. Let L_0 be the characteristic length, ρ_0 the characteristic density, χ_{i0} the characteristic ionization, and v_0 the characteristic velocity; for subsonic flows, we set v_0 equal to the isothermal sound speed, c_s. Denote the corresponding dimensionless quantities by $\mathbf{x}^* \equiv \mathbf{x}/L_0$ (where $\mathbf{x}$ is position), $t^* \equiv v_0 t/L_0$, and $\rho^* \equiv \rho/\rho_0$. We define the dimensionless field strength as

$$B^* \equiv \frac{B}{B_0} \equiv \frac{B}{(8\pi\rho_0)^{1/2} v_0}, \tag{26}$$

where we have included a factor $(8\pi)^{1/2}$ for convenience. The dimensionless coupling constant is

$$\gamma_0^* \equiv \left(\frac{\rho_0 L_0}{v_0}\right)\gamma_0 \rightarrow 2.16 \times 10^5 \left(\frac{N_{\rm H}}{10^{20}\ {\rm cm}^{-2}}\right)\left(\frac{1\ {\rm km\ s}^{-1}}{v_0}\right), \tag{27}$$

where we have used the numerical values cited above. The characteristic value of the ambipolar diffusion velocity is then

$$v_{\rm AD,0} = \frac{B_0^2}{4\pi\gamma_0\chi_{i0}\rho_0^2 L_0} = \frac{2v_0}{\chi_{i0}\gamma_0^*}. \tag{28}$$

The corresponding characteristic value for the magnetic Reynolds number for ambipolar diffusion is

$$R_{\rm AD,\,0} = t^*_{\rm AD,\,0} = \frac{1}{v^*_{\rm AD,\,0}} = \frac{1}{2}\chi_{i0}\gamma_0^*. \tag{29}$$

The other dimensionless parameters that characterize simple MHD problems are the plasma β,

$$\beta \equiv \frac{\rho c_s^2}{B^2/8\pi} = \frac{\rho^* c_s^{*2}}{B^{*2}}, \tag{30}$$

(recall that $c_s^* = c_s/v_0$ for supersonic flows and $c_s^* = 1$ for subsonic ones); the Mach number $\mathcal{M} = v^*/c_s^*$; and the Alfvén Mach numbers

$$\mathcal{M}_A = \left(\frac{\rho^*}{2}\right)^{1/2}\frac{v^*}{B^*}, \qquad \mathcal{M}_{Ai} = \left(\frac{\rho_i^*}{2}\right)^{1/2}\frac{v_i^*}{B^*}. \tag{31}$$

2.4. Numerical method for two-fluid MHD

Based on a stable semi-implicit treatment of the ion momentum equation in Tóth (1995), Mac Low & Smith (1997) modified the treatment and implemented a 2-fluid approach ambipolar diffusion calculation into the ZEUS code. We implement the same 2-fluid algorithm into the ZEUS-MP code, which is a multi-physics, massively parallel, message-passing implementation of the ZEUS code (Hayes et al. 2005). The Courant timestep for ambipolar diffusion will be determined by $\Delta x/v_{Ai}$. Therefore, using this algorithm, the Courant timestep size is proportional to the root of the ionization fraction, $x_i^{1/2}$. For an ionization fraction of 10^{-4}, the timestep size of the simulation

will be 100 times smaller than the hydrodynamic timestep size. For core collapse problem in the star formation theory, x_i could be as small as 10^{-8}. Simulating such systems is not feasible at the present time. In the following tests, we use a fix Courant number of 0.5.

Numerical diffusion has similar effect on magnetic field diffusion as ambipolar diffusion. In ZEUS-MP, the HSMOCCT scheme (Hawley & Stone 1995; Hayes et al. 2005) is adopted in the MHD module, which makes the code more robust when applied to fully multidimensional problems characterized by strong magnetic discontinuities. Because of that, ZEUS-MP requires twice as many zones to get the same level of accuracy as with ZEUS-2D. Therefore, in some cases, strong magnetic discontinuities could need as many as 6 zones to be resolved. In all the following tests, the ambipolar diffusion length scale is at least an order of magnitude larger than the numerical diffusion scale.

2.5. Heavy-ion approximation for ambipolar diffusion

To circumvent the small timestep difficulty, we can increase the ionization fraction and at the same time reduce the collisional coupling constant γ between the ions and neutrals so that $\rho_i\gamma \propto \chi_{i0}\gamma_0 =$ constant. We term this the "heavy-ion approximation." Because of the much larger ion density, the timestep size determined by the Courant condition for the ions will be significantly increased. The MHD equations for the neutrals (eqs. 1 and 3) and for the magnetic field in the limit of weak ionization (eqs. 6 and 14) will remain the same under this transformation. The ion equation of motion is altered by this change, however. Correspondingly, all the dimensionless parameters that characterize an MHD problem in a weakly ionized, isothermal plasma (including the ambipolar diffusion Reynolds number and time scale, $R_{\rm AD,\,0} = t^*_{\rm AD,\,0} \propto (\chi_{i0}\gamma_0)$—eq. 29) are unaffected by this transformation, with the exception of the ion Alfvén Mach number $\mathcal{M}_{Ai}$. In weakly ionized astrophysical plasmas, the ion Alfvén Mach number $\mathcal{M}_{Ai}$ is generally very small. As we shall see, the heavy-ion approximation begins to break down when $\mathcal{M}_{Ai}$ approaches unity. Oishi & Mac Low (2005) have independently used the heavy-ion approximation for simulations of 2-fluid turbulence, although they did not justify it. They adopted a very large ionization fraction of 0.1 in order to speed up the calculation by a large factor. In the following, we present three test problems using our modified ZEUS-MP code, named ZEUS-MPAD, to uncover the conditions under which the heavy-ion approxmation can be used to accelerate ambipolar diffusion simulations with reasonable accuracy. As we are going to test models with different ion densities, it is more direct to refer to the models in terms of the ratio of the ion density used in the simulation to the physical ion density,

$$\mathcal{R} = \frac{\rho_{i,\,\rm sim}}{\rho_{i,\,\rm phys}} = \frac{\chi_{i0,\,\rm sim}}{\chi_{i0,\,\rm phys}} = \frac{\mathcal{M}^2_{Ai,\,\rm sim}}{\mathcal{M}^2_{Ai,\,\rm phys}}. \tag{32}$$

Since the time step varies as $\chi_i^{1/2}$, the heavy-ion approximation accelerates ambipolar diffusion calculations by a factor $\mathcal{R}^{1/2}$.

3. Tests

3.1. C-type Shock Formation

The first test of our ZEUS-MPAD code is the formation of a C-shock. Due to the presence of an interstellar magnetic field and the partially ionized gas, a strong J-type shock in molecular clouds will evolve into C-type shock structure due to ambipolar diffusion (e.g. Draine 1980; Chernoff 1987; Draine & McKee 1993). The formation of C-type shocks is usually cited to explain the survival of molecules in high velocity shocks and has become a standard 2-D test for ambipolar diffusion algorithms (Mac Low et al. 1995; Smith & Mac Low 1997). We follow Smith & Mac Low (1997) in starting with a highly super-Alfvénic J-shock moving at 50 km s^{-1} into a medium with an Alfvén velocity of 2 km s^{-1}, corresponding to an Alfvén Mach number $\mathcal{M}_A = 25$. Since we are interested in the overall structure of the shock, and not its emission, we follow Smith & Mac Low (1997) and assume that the gas is isothermal with a negligible thermal pressure ($c_{\rm s} = 0.01$ km s^{-1}). The initial number density of H atoms is $n_{\rm H} = 10^5$ cm^{-3}, and the ionization fraction is $x_i = 10^{-6}$. Following Mac Low & Smith (1997), we shall set the ion mass $m_{\rm i} = 10 m_{\rm H}$, and the neutral mass $m_n = 7/3 m_{\rm H}$ (assuming 10% He) so that $\gamma_0 = 9.21 \times 10^{13}$ cm^3 g^{-1} s^{-1}; we also follow their lead in setting $\gamma = \gamma_0$, neglecting the velocity dependence of the coupling that sets in above about 20 km s^{-1}.

For $\chi_i \ll 1$ and negligible thermal pressure, the shock jump conditions give

$$\rho_n v_n = \rho_0 v_s, \tag{33}$$

$$\frac{B}{\rho_i} = \frac{B_1}{\rho_{i,1}}, \tag{34}$$

$$\frac{\rho_0}{\rho_n} + \frac{B^2}{8\pi\rho_0 v_s^2} = 1 + \frac{1}{2\mathcal{M}_A^2}, \tag{35}$$

where quantities ahead of the shock are labeled with a subscript "1," and we have set the characteristic density $\rho_0 = \rho_1$ and the characteristic velocity equal to the shock velocity, $v_0 = v_s$. Note that for highly super-Alfvénic shocks, the post-shock magnetic field (labeled by the subscript "2") is given by $B_2^2 = 8\pi\rho_0 v_s^2$ and that $B_1 = B_2/(\sqrt{2}\mathcal{M}_A)$.

Since the ions decelerate well before the neutrals, the ion equation of motion becomes (Wardle 1990)

$$-\frac{d}{dx}\,\frac{B^2}{8\pi} = \gamma_0 \rho_n \rho_i (v_i - v_n) \simeq -\gamma_0 \rho_n \rho_i v_n. \tag{36}$$

Using the shock jump conditions, this simplifies to

$$\frac{dB}{dx} = \frac{4\pi\gamma_0 \rho_{i,1} \rho_0 v_s}{B_1}, \tag{37}$$

which can be readily integrated to give the shock thickness (Wardle 1990),

$$L_s = \frac{B_1 B_2}{4\pi\gamma_0 \rho_{i,1} \rho_0 v_s}, \tag{38}$$

$$= \sqrt{2} v_{A,1} t_{ni,1}, \tag{39}$$

$$= 2 v_s t_{ni,2}, \tag{40}$$

where we assumed $\mathcal{M}_A \gg 1$ and used the jump conditions to derive the second and third expressions. The final expression states that the shock thickness is about equal to the distance that the shock travels in the time it takes for a neutral to hit an ion after the ions are compressed (recall that the ions compress well ahead of the neutrals). This shock thickness is in excellent agreement with the numerical results described below. Note that the shock thickness is just the ambipolar diffusion length introduced in equation (17) above,

$$\ell_{\rm AD} = \frac{1}{4\pi\gamma_0} \left(\frac{B}{\rho_i} \right) \frac{B}{\rho_n v}. \tag{41}$$

Evaluating B/ρ_i upstream, noting that $\rho_n v = \rho_0 v_s$, and setting the final factor of $B = B_2$ since we want $\ell_{\rm AD}$ for the entire shock, we find that this expression is identical to that in equation (39). Correspondingly, this implies that the ambipolar diffusion Reynolds number for the shock is $R_{\rm AD}(L_s) = 1$.

For the adopted initial conditions, the neutral-ion collision time ahead of the shock is $t_{ni,1} = 1/\gamma\rho_i \simeq 200$ yr, and the thickness of the C-type shock is $L_s \simeq 1.8 \times 10^{15}$cm. We ran the simulation on a $256 \times 16 \times 16$ grid, with the physical domain size equivalent to a resolution in which the C-type shock width is resolved by 120 cells, denoted L120 in Mac Low & Smith (1997). In Figure 1, we show the velocities of the ions and neutrals of the steady state C-type shock after integrating for a time t_{ni}.

In order to find out how much we can increase the ionization fraction and still have an accurate C-type shock structure, we ran four other shock models with $\mathcal{R} = 10$, 10^2, 10^3, and 10^4. The collisional coupling constant is modified accordingly such that the numeric value $\mathcal{R}\,\gamma = 9.21 \times 10^{13}$. The velocities of the ions and neutrals calculated using ZEUS-MPAD are shown in Figure 2. These velocities are almost identical for $\mathcal{R} = 1$ and 10 but for $\mathcal{R} = 10^4$, the velocity of the neutrals is clearly shifted to the right by almost $0.1 L_{\rm shock}$. In Figure 3, we show the differences of ion velocities of each model using the physical model $\mathcal{R} = 1$ as reference. We can see very large errors in the ion velocity when $\mathcal{R} = 10^4$. In order to quantify the error in the velocity, we define

$$\mathrm{err}(v) = \int_{L_s} \frac{|v_{\mathcal{R}} - v_1|}{|v_1|} dx, \tag{42}$$

with the ionization ratio $\mathcal{R}$ as a subscript; the region L_s for the integration extends from the beginning of the shock front in the neutrals to the end of the ion shock front. Table 1 gives $\mathrm{err}(v)$ as a function of the ionization ratio $\mathcal{R}$ and the corresponding initial ion Alfvén Mach number for all the models listed. Note that when the ion Alfvén Mach number $\mathcal{M}_{A,i} \lesssim 0.5$, the velocity error is less than 1%. When $\mathcal{M}_{A,i} \lesssim 0.5$, the criterion in equation (25) is approximately satisfied, since $R_{\rm AD}(L_s)$=1 in this test. In Figures 4 and 5, we show the calculated profiles of the magnetic field and the magnetic field error profiles for different values of $\mathcal{R}$. The error in B is defined in the same

manner as the velocity error and is listed in Table 1. The conclusions from Figures 4 and 5 are similar to those in Figures 2 and 3. For the model $\mathcal{R} = 10^4$, the magnetic field near the upstream of the shock has a very large error. From the comparison, we conclude that when the ion velocity is super-Alfvénic, a shock is formed in the ion component and large errors occur in the magnetic field as well as in the neutral velocity. So long as the ions remain sub-Alfvénic in the simulation, the heavy-ion approximation is quite accurate. In typical cases, this permits one to accelerate the simulation by a factor $\mathcal{R}^{1/2} \sim 30$.

3.2. Wardle Instability

Our second test of the ZEUS-MPAD code is the Wardle instability, which occurs in C-type shocks (Wardle 1990). This instability occurs because when the magnetic field is slightly buckled, ions will be forced into the valleys of the field lines by the drag force of the neutrals. As ions accumulate in the field-line valleys, the valleys will be further deepened, and the growth exponentiates (see Figure 1 in Mac Low & Smith 1997). Mac Low & Smith (1997) studied the Wardle instability in both 2-D and 3-D using their modified ZEUS code. The smallest ionization fraction that they used in their simulations was 10^{-4}. With such an ionization fraction, they pointed out that the calculation became very expensive, with $\gg 10^5$ cycles per neutral-ion collision time. It becomes totally impractical to simulate even smaller ionization fractions.

Here we perform the same Wardle instability calculation using the heavy-ion approxmation to determine if we can reproduce the instability with a much faster calculation. Following Mac Low & Smith (1997), we use a steady-state, isothermal C-type shock as the initial condition for the Wardle instability test, with a 10^{-6} cell-by-cell perturbation to the neutral density. For a physical ionization fraction of 10^{-6}, this calculation would require several times 10^6 cycles per neutral-ion collision time. By choosing $\mathcal{R} \gg 1$, we can speed up the calculation many times. We performed two simulations using a $256 \times 96 \times 96$ grid with $\mathcal{R} = 10^4$ and 10^2. The resolution of the simulations is equivalent to L120 in Mac Low & Smith (1997), as explained in §3.1. For the simulation with $\mathcal{R} = 10^4$, the ions are super-Alfvénic with Alfvén Mach number $\mathcal{M}_{A,i} \sim 5$. The criterion in equation (25) will be seriously violated as $R_{\rm AD}(L_s)$=1 in this test. We expect this simulation to have significant differences in the instability growth rate as compared to the analytical solution because the shock will become J-type. Note that Wardle (1990) pointed out that J-type shocks with $v_s \lesssim 100$ km s^{-1} would still be unstable. In the second simulation with $\mathcal{R} = 10^2$, the ions are sub-Alfvénic and the Alfvén Mach number $\mathcal{M}_{Ai} \sim 0.5$. The criterion in equation (25) is satisfied. During the whole calculation, the ratio $\mathcal{M}_{A,i}^2/R_{\rm AD}(L_s)$ is never larger than the initial ratio along the whole shock length, and as a result the condition for ignoring the ion inertia is satisfied throughout the simulation. We use the growth rate of magnetic pressure in the flow direction, B_x^2, normalized by the initial magnetic pressure, $B_{y,0}^2$, to measure the instability growth rate.

In Figure 6, we plot $B_x^2/B_{y,0}^2$ for these two simulations as a function of time. For $\mathcal{R} = 10^4$, the inferred growth rate is $s = 22.8 t_{ni}^{-1}$, whereas for $\mathcal{R} = 10^2$, it is $s = 44.1 t_{ni}^{-1}$. The instability growth

rate from the analytic solution is $s = 42.5 t_{ni}^{-1}$ (Mac Low & Smith 1997). As we expected, the $\mathcal{R} = 10^2$ calculation is in good agreement with the analytic result, but not the $\mathcal{R} = 10^4$ simulation. Figures 7a and 7b show slices of the density and velocity of the neutrals for the $\mathcal{R} = 10^2$ model at $t = 0.54 t_{ni}$. The instability is well developed at $t = 0.54 t_{ni}$ in this sub-Alfvénic case, with clear spiking features. We stop the calculation at $t = 0.54 t_{\rm ni}$ because the instability becomes non-linear. For the super-Alfvénic case, the amplitude of the instability is still small at $t = 0.54 t_{ni}$ (Figures 7c and 7d), but is nonlinear by $t = 1.08 t_{ni}$ (Figures 7e and 7f). These instability tests confirm that the ion Alfvén Mach number $\mathcal{M}_{Ai} \lesssim 0.5$ is a good criterion for choosing an appropriate value of $\mathcal{R}$ in the heavy-ion approxmation.

3.3. 1-D Self-gravitating Ambipolar Diffusion Collapse

The final test of our ZEUS-MPAD code is the 1-D self-gravitating collapse with ambipolar diffusion first formulated by Shu (1983). Mac Low et al. (1995) used this test for their ambipolar diffusion implementation but did not include direct comparison to the solutions in Shu (1983). We shall see that although the final equilibrium solution to this problem depends explicitly on the ion mass (see the Appendix), the heavy-ion approxmation generally works well until the solution begins to approach the final equilibrium. Consider a partially ionized, magnetized medium stratified in plane-parallel layers normal to the $z-$axis. The magnetic field is, say, in the x-direction, and the medium is initially in hydrostatic equilibrium. We assume that the ambipolar diffusion time is large compared to the dynamical time ($t^*_{\rm AD,\,0} \gg 1$), so that the evolution is quasi-static; as a result, we can neglect the inertial terms in the equation of motion. As usual, we neglect the velocity dependence of the ion-neutral coupling, so that $\gamma = \gamma_0$. Recall that we are assuming that the gas is weakly ionized ($\rho_i \ll \rho_n \simeq \rho$). Following Shu (1983), we assume that the ionization is sufficiently small that we can neglect the weight of the ions also; this approximation breaks down high above the midplane, as discussed in the Appendix. Let

$$\sigma_n \equiv \int_0^z \rho_n \left(z', t\right) dz', \tag{43}$$

be the surface density of the neutrals; in differential form, this is

$$\frac{\partial z}{\partial \sigma_n} = \frac{1}{\rho_n}. \tag{44}$$

The gravitational acceleration is then $g = -4\pi G\sigma \simeq -4\pi G\sigma_n$. Following Shu (1983), we set our characteristic length and density to be

$$L_0 = \frac{c_s^2}{2\pi G \sigma_{n\infty}} \tag{45}$$

$$\rho_0 = \frac{2\pi G \sigma_{n\infty}^2}{c_s^2}, \tag{46}$$

so that $\rho_0 L_0 = \sigma_{n\infty}$, where $\sigma_{n\infty}$ is the total neutral surface density from the midplane to infinity. For the remainder of this section, we shall use dimensionless quantities and omit the superscript " * " for simplicity. The total neutral surface density is then $\sigma_{n\infty} = 1$ and the gravitational acceleration is $g = -2\sigma$. Our assumption that the ion-neutral coupling is constant implies $\gamma = \gamma_0$. The continuity equation for the neutrals (eq. 1), the summed equations of motion for the neutrals and ions (eq. 3 + eq. 4), and the induction equation (eq. 14) then become

$$\frac{\partial \rho_n}{\partial t} + \rho_n^2 \frac{\partial v_n}{\partial \sigma_n} = 0 \tag{47}$$

$$\frac{\partial}{\partial \sigma_n}\left(\rho_n + B^2\right) = -2\sigma_n \tag{48}$$

$$\frac{1}{\rho_n}\frac{\partial B}{\partial t} + B\frac{\partial v_n}{\partial \sigma_n} = \frac{\partial}{\partial \sigma_n}\left(\frac{\chi_{i0} B^2}{t_{\mathrm{AD},\,0}\,\rho_i}\frac{\partial B}{\partial \sigma_n}\right), \tag{49}$$

where it should be noted that $\partial/\partial t$ evaluated at constant σ_n is the same as the convective derivative $d/dt = \partial/\partial t + v_n \partial/\partial z$. Since ρ_i/χ_{i0} and $t_{\mathrm{AD},\,0}$ are independent of the ionization, we refer to these as the "$\chi_{i0} \to 0$" equations. The equation of motion is readily integrated to give

$$\rho_n + B^2 = 1 - \sigma_n^2. \tag{50}$$

The remaining two equations yield

$$\frac{\partial}{\partial \tau}\frac{B}{\rho_n} = \frac{\partial}{\partial \sigma_n}\left(\frac{\chi_{i0} B^2}{\rho_i}\frac{\partial B}{\partial \sigma_n}\right), \tag{51}$$

where $\tau \equiv t/t_{\mathrm{AD},\,0}$ is the time normalized to the characteristic ambipolar diffusion time; with the value of χ_{i0} specified in §3.3.1 below, it is identical to the τ introduced by Shu (1983).

3.3.1. Equilibrium ionization

Shu (1983) assumed that the ions are in ionization equilibrium, and as a result he did not need to solve the momentum equations for the ions and the neutrals separately. He was therefore able to reduce the problem to solving equations (43), (50), and (51). He approximated the ionization as

$$\rho_{i,\,\mathrm{phys}} = C\rho_n^{1/2}. \tag{52}$$

In our notation C is dimensionless, with a numerical value of $3 \times 10^{-16}/\rho_0^{1/2}$; for example, setting $\rho_0 = 10^{-18}$ g cm^{-3} (which Shu 1983 adopts as a typical value at the center of a dense core) gives $C = 3 \times 10^{-7}$. Recall that χ_{i0} is the characteristic value of ρ_i. When ρ_i is a function of ρ_n, as in this case, we set $\chi_{i0} = \rho_i(\rho_n = 1)$; hence, $\chi_{i0,\,\mathrm{phys}} = C$. In simulations, we increase χ_{i0} by a factor $\mathcal{R}$, so that $\chi_{i0} = C\mathcal{R}$. The factor χ_{i0} enters only into the induction equation (51), but the dependence on $\mathcal{R}$ cancels:

$$\frac{\rho_i}{\chi_{i0}} = \frac{\rho_{i,\,\mathrm{phys}}}{\chi_{i0,\,\mathrm{phys}}} = \frac{C\rho_n^{1/2}}{\chi_{i0,\,\mathrm{phys}}} = \rho_n^{1/2}, \tag{53}$$

since $\chi_{i0,\,\mathrm{phys}} = C$. As a result, the induction equation becomes

$$\frac{\partial}{\partial\tau}\left(\frac{B}{\rho_n}\right) = \frac{\partial}{\partial\sigma}\left(\frac{B^2}{\rho_n^{1/2}}\frac{\partial B}{\partial\sigma}\right), \tag{54}$$

which is identical in form to Shu's equation.

3.3.2. Ion conservation

ZEUS-MPAD is a two-fluid code in which each fluid is conserved; it is therefore not possible to impose ionization equilibrium in the existing ZEUS-MPAD code except as an initial condition. Since the magnetic flux is frozen to the ions we have $\rho_i \propto B$ for this one-dimensional problem. We define C_B by

$$\frac{\rho_i}{\chi_{i0}} = \frac{\rho_{i,\,\mathrm{phys}}}{\chi_{i0,\,\mathrm{phys}}} \equiv C_B B, \tag{55}$$

where C_B is independent of time. The induction equation then becomes

$$\frac{\partial}{\partial\tau}\left(\frac{B}{\rho_n}\right) = \frac{\partial}{\partial\sigma}\left(\frac{B}{C_B}\frac{\partial B}{\partial\sigma}\right). \tag{56}$$

We adopt the same initial conditions as in Shu (1983): the magnetized plasma is initially in hydrostatic equilibrium with the magnetic pressure proportional to the gas pressure (i.e., the plasma β is a constant, β_0, which is the inverse of Shu's α_0):

$$\rho_n = \frac{\beta_0}{1+\beta_0}\mathrm{sech}^2\left(\frac{z\beta_0}{1+\beta_0}\right), \tag{57a}$$

$$B = \left(\frac{1}{1+\beta_0}\right)^{1/2}\mathrm{sech}\left(\frac{z\beta_0}{1+\beta_0}\right), \tag{57b}$$

$$\sigma = \tanh\left(\frac{z\beta_0}{1+\beta_0}\right). \tag{57c}$$

We also assume that the ionization is initially in equilibrium, so that $\rho_i(t=0) = \chi_{i0}[\rho_n(t=0)]^{1/2}$. We then have (see eq. 30)

$$\beta_0 = \frac{\rho_n}{B^2} = \frac{(\rho_i/\chi_{i0})^2}{B^2} = C_B^2, \tag{58}$$

where ρ_n, etc., are evaluated at the initial instant. Thus the quantity C_B is independent of position as well as being constant in time. Comparing with Shu (1983), we see that the only difference in the three equations to be integrated is the new induction equation (56). We use a finite difference scheme to integrate equations (44), (50), and (56) with 40, 80, 160, and 320 equally spaced cells in σ for a convergence study. Our convergence study on the difference scheme shows that when we have 80 cells, the error is already less than 0.6%. To compare with ZEUS-MPAD calculation, we shall use the results from the 320-cell integration. We set the timestep $\Delta t = \Delta\sigma^2$ for numerical

stability. As Shu (1983) did, we choose $\beta_0 = 1$. To test the idea of modifying the ion density and collisional coupling constant, we use ZEUS-MPAD to run the same problem on 3 models with $\mathcal{R} = 3.33 \times 10^4$, 333, and 33.3. The value of γ_0 is adjusted accordingly. For direct comparison, we adopt $\gamma_0 = 3.5 \times 10^{13}$ cm^3 g^{-1} s^{-1} (Shu 1983). The neutral density, magnetic field, and vertical dimension are initialized according to equations (57a)–(57c). The ion density is initialized such that $\rho_i = \chi_{i0}\rho_n^{1/2}$. The system is initially at rest. The maximum vertical height is $z = 40$, and the calculation is performed using a $16 \times 16 \times 512$ grid. Figure 8 compares the results from the 320-cell integration of the $\chi_{i0} \rightarrow 0$ equations with the ZEUS-MPAD simulation with $\mathcal{R} = 33.3$. For the period of time shown, the simulation with $\mathcal{R} = 33$ agrees extremely well with the 320-cell integration. This is to be expected: since $\mathcal{M}_{A,i} \sim 2.6 \times 10^{-4}$ is much less than $R_{\rm AD}(\ell_{vi}) \sim 0.6$ at the characteristic height, the criterion in equation (25) is well satisfied. For sufficiently late times, however, the simulation will differ from the integration of the $\chi_{i0} \rightarrow 0$ equations as the effects of the finite ion mass become important. As shown in the Appendix, the field diffuses out of the neutrals until it reaches an equilibrium value, $B_{\rm final}$, which is set by the weight of the ions. The effect of finite ion mass is apparent in Figure 9, which compares the $\chi_{i0} \rightarrow 0$ results with ZEUS-MPAD simulations at $\mathcal{R} = 3.33 \times 10^4$ and 333. Such large values of $\mathcal{R}$ are desirable in order to significantly accelerate the calculation. We find that the heavy-ion approxmation remains accurate to better than 5% until $B < 3B_{\rm final}$ for the values of $\mathcal{R}$ we have considered. Note that at sufficiently large heights, the magnetic field actually increases with time ($B_{\rm final} > B_{\rm initial}$), and the ionization approximation is never valid there.

4. Discussion and Conclusions

Ambipolar diffusion governs the drift of ions across the magnetic field in many astrophysical problems, such as C-type shocks and star formation. Since cloud cores evolve deep inside molecular clouds, where the ionization fraction is very small, ideal MHD calculations cannot accurately describe the core collapse process, and we must treat the ion and neutral components separately. In the standard theory of star formation (Shu, Adams, & Lizano 1987), the time scale for star formation is determined by the time scale of the ambipolar diffusion. The question as to whether dense cloud cores are magnetically sub-critical or super-critical is under debate. Observationally, both magnetically sub-critical and super-critical dense cloud cores are observed (e.g. Crutcher 2005). For magnetically sub-critical cores, ambipolar diffusion is likely to be essential in permitting the core to collapse. Even for magnetically super-critical cores, ambipolar diffusion retards the collapse. In either case, it could play a major role in reducing the magnetic flux to the small values it has in the stars that form (Mouschovias 1987).

Unfortunately, simulations using specially designed semi-implicit algorithms to study the core collapse process are still greatly limited by the very small timestep imposed by the stiff term in the momentum equations introduced by ambipolar diffusion. For a simple 2-fluid shock calculation with an ionization fraction of 10^{-4}, it will take many times 10^5 cycles to complete one simulation

using the approach of Mac Low & Smith (1997), for example. At present, it is totally infeasible to simulate the 3D core collapse process with an ionization fraction of 10^{-8} using this approach. Some other semi-implicit or fully implicit methods may allow significantly larger timesteps (e.g., Falle 2003) but involve complex code development. Therefore, there has not been much progress on 3D simulations with ambipolar diffusion up to this point.

In this paper, we have investigated a method of significantly accelerating ambipolar diffusion calculations by simultaneously increasing the ion density and reducing the ion-neutral collisional coupling constant so that the ambipolar diffusion time is unaffected. We term this the "heavy-ion approxmation." This approximation has the advantage of being straightforward to implement, and has been used independently by Oishi & Mac Low (2005). We performed three groups of tests in order to assess the accuracy of this approximation: (1) C-type shock formation, (2) Wardle instability, and (3) one-dimensional collapse. From the tests, we conclude that there are two restrictions on the application of the heavy-ion approxmation for ambipolar diffusion: First, for dynamical problems in which the ion Alfvén Mach number $\mathcal{M}_{Ai}$ is small (i.e., the ion inertia is negligible), it is essential to restrict the increase in the ion density so that $\mathcal{M}^2_{Ai,\,\mathrm{sim}} \ll R_{\mathrm{AD}}(\ell_{vi})$ throughout the course of the calculation. The problems considered here have $R_{\mathrm{AD}}(\ell_{vi}) \sim 1$, and we have found that keeping $\mathcal{M}_{Ai,\,\mathrm{sim}} < \frac{1}{2}$ leads to reasonably accurate results, with errors of $< 1\%$ (see Table 1). This condition limits the factor by which the ionization can be increased, $\mathcal{R}$, to (eq. 32)

$$\mathcal{R} \leq \frac{R_{\mathrm{AD}}(\ell_{v_i})}{4\mathcal{M}^2_{Ai}} \sim \frac{1}{4\chi_{i0}\mathcal{M}^2_A}. \tag{59}$$

As remarked in §2.1, the condition $\mathcal{M}^2_{Ai,\,\mathrm{sim}} \ll R_{\mathrm{AD}}(\ell_{vi})$ can be very stringent for flows with large fluctuations, such as turbulent flows. Second, for quasi-static problems in which the ion inertia is negligible due to small velocities, it is necessary that other terms dependent on the ion mass, such as the gravitational force on the ions, remain negligible. For the particular case of the collapse of a 1D self-gravitating slab, we found that the heavy-ion approxmation was accurate so long as the value of the magnetic field remained at least about 3 times the final equilibrium value, which was determined by the ion mass. We conclude that, when these conditions are satisfied, the heavy-ion approxmation should be able to accelerate 3D simulations of ambipolar diffusion–driven core collapse by factors of $10^2 - 10^3$, depending on the problem.

In our investigation, we have used the ion conservation assumption for all three tests. In reality, one would like to use equilibrium ionization for systems with slow evolution compared to ionization and recombination timescales. When ionization and recombination rates are in balance, the ion density often has a power-law dependence on the neutral density, which is commonly used in 1-fluid ambipolar diffusion calculations (e.q. Shu 1983; Fiedler & Mouschovias 1992; Mac Low et al. 1995). Note that the calculation of the actual ionization is complicated, and that significant deviations from equilibrium can occur in dynamically evolving clouds (Lintott & Rawlings 2006). If one uses a power-law form for the ion density, or includes ionization and recombination rates in determining ion density, it is equivalent to including a source term in the mass, momentum and

energy equations for the ions and neutrals. However, so long as the ion inertia is small, the heavy ion approximation still applies for the case of time-dependent ionization.

We also assume isothermality in our study. The isothermal assumption is generally valid when the neutral number density is less than 10^9 cm^{-3}. For problems with higher density or when the isothermal assumption is no longer valid, one would need to include the energy equations with relevant heating and cooling terms, such as heating due to ambipolar diffusion (e.g. Padoan, Zweibel, & Nordlund 2000) and viscous heating. For ambipolar diffusion heating, the heating rate $\Gamma_{\rm AD} = \gamma\rho_i\rho_n|v_i - v_n|^2$ (Shu 1992). By keeping $\gamma\rho_i$ constant in the heavy ion approximation, the heating due to ambipolar diffusion drift will remain the same.

We acknowledge helpful conversations with Robert Fisher. This work was supported in part by the NASA ATP grant NAG5-12042, by an NSF grant of computer time at SDSC, and by a DOE grant of computer time at NERSC. The research of CFM is supported in part by NSF grants AST-0098365 and AST-0606831 , and that of RIK is done in part under the auspices of the US Department of Energy at the Lawrence Livermore National laboratory under contract W–7405–Eng–48with University of California.

A. AMBIPOLAR DIFFUSION IN SELF-GRAVITATING LAYERS WITH "HEAVY" IONS

In §3.3, we tested the heavy-ion approxmation for ambipolar diffusion calculations with the problem of a self-gravitating slab. Following Shu (1983), we ignored the effects of gravity on the ions because ionization fraction was assumed to be small. (Note, however, that ZEUS-MPAD does include the effects of gravity on the ions.) The solution to this ambipolar diffusion problem shows that at large heights above the midplane, the ionization fraction becomes significant and the effects of gravity on the ions must be included. In this Appendix, we determine the final equilibrium when the ions are included. We use the dimensionless quantities defined in §3.3, and as in that section we omit the superscript " * " for simplicity. We assume that initially the slab is ionization equilibrium, so that $\rho_i = \chi_{i0}\rho_n^{1/2}$ at the initial instant. With the initial ρ_n given by equation (57a), the total column of ions is then

$$\sigma_{i\infty} = \frac{\pi}{2}\left(\frac{1+\beta_0}{\beta_0}\right)^{1/2}\chi_{i0}. \tag{A1}$$

As discussed in the text, we assume that this is constant in time. In the final equilibrium, there is no relative velocity, so the magnetic field cannot exert any indirect force on the neutrals. If the plasma is initially weakly ionized, the final state of the neutrals is given to good accuracy by

$$\rho_n = \mathrm{sech}^2 z. \tag{A2}$$

The final state of the ions is given by the ion equation of motion with $v = 0$:

$$\frac{d}{dz}\left(B^2 + \rho_i\right) = \rho_i g. \tag{A3}$$

Recall that $g = -2\sigma$ in our dimensionless notation. We focus on the region high above the midplane ($z \gg 1$), where $\sigma \simeq 1$. Equation (A3) can then be immediately integrated to give

$$B^2 + \rho_i = 2(\sigma_{i\infty} - \sigma_i). \tag{A4}$$

Recall that (eq. 55)

$$\rho_i = \chi_{i0} C_B B = \chi_{i0} \beta_0^{1/2} B. \tag{A5}$$

One can readily show that for $\chi_{i0}\beta_0 \ll 1$, the magnetic pressure dominates the thermal pressure of the ions unless σ_i is very close to $\sigma_{i\infty}$. Equations (A4) and (A5) then imply

$$\frac{d\sigma_i}{dz} = \rho_i \simeq \chi_{i0}(2\beta_0)^{1/2}(\sigma_{i\infty} - \sigma_i)^{1/2}, \tag{A6}$$

which can be integrated to give

$$1 - \frac{\sigma_i}{\sigma_{i\infty}} \simeq \left(1 - \frac{z}{z_m}\right)^2, \tag{A7}$$

where

$$z_m \equiv \frac{a}{(\beta_0 \chi_{i0})^{1/2}}, \tag{A8}$$

with

$$a^2 \equiv \frac{2\sigma_{i\infty}}{\chi_{i0}} = \pi \left(\frac{1+\beta_0}{\beta_0}\right)^{1/2}. \tag{A9}$$

The final values of the magnetic field and ion density are then given by

$$B_{\rm final} \simeq a\chi_{i0}^{1/2}\left(1 - \frac{z}{z_m}\right), \tag{A10}$$

$$\rho_{i,\,\rm final} \simeq a\beta_0^{1/2}\chi_{i0}^{3/2}\left(1 - \frac{z}{z_m}\right). \tag{A11}$$

In this approximation, the magnetic field and ion density vanish at $z = z_m$; in fact, at z_m the thermal pressure of the ions begins to dominate the magnetic pressure and the field and the ion density decline exponentially above that point. In the midplane, the field has declined by a factor of order $\chi_{i0}^{1/2}$ from its initial value, and the scale height has correspondingly increased by a factor $\chi_{i0}^{-1/2}$. Shu (1983) neglected the mass of the ions since he was interested in the limit of very small ionization; his solution therefore corresponds to the limit $\chi_{i0} \to 0$. In §3.3, we discussed the effects on the solution of the 1-D ambipolar diffusion collapse problem when using a large ion mass ratio χ_{i0} (see Figure 9). To verify that the ZEUS-MPAD results presented in Figure 9 are correct, we can directly compare the ZEUS-MPAD results with equations (A10) or (A11). In Figure 10 the densities of neutrals and ions from equations (A2) and (A11), respectively, are plotted together with the densities of ions and neutrals from the $\mathcal{R} = 3.33 \times 10^4$ model using ZEUS-MPAD at $\tau = 20$. The ion densities from the ZEUS MP-AD calculation at $\tau = 5$ and 10 are also plotted. The two sets of results match very well; at the largest heights, where the ion densities are discrepant, the ZEUS-MPAD results are converging toward the analytic solution.

REFERENCES

Basu, S. & Mouschovias, T. Ch. 1994, ApJ, 432, 720

Bergin, E. A., Plume, R., Williams, J. P., & Myers, P. C. 1999, ApJ, 512, 724

Brandenburg, A. & Zweibel, E. G. 1994, ApJ, 427, 91

Caselli, P., Walmsley, C. M., Tervieza, R., & Herbst, E. 1998, ApJ, 499, 234

Caselli, P., Walmsley, C. M., Zucconi, A., Tafalla, M., Dore, L., & Myers, P. C. 2002, ApJ, 565, 344

Chernoff, D. F. 1987, ApJ, 312, 143

Crutcher, R. M. 2005, in The Magnetized Plasma in Galaxy Evolution, Proceedings of the conf. held in Krakow, ed. K. T. Chyzy, K. Otmianowska-Mazur, M. Soida, and R. J. Dettmar (Jagiellonian Univ.), p. 103

Draine, B. T. 1980, ApJ, 241, 1021

Draine, B.T., Roberge, W.G., & Dalgarno, A. 1983, ApJ, 264, 485

Draine, B. T. & McKee, C. F. 1993, ARA&A, 31, 373

Falle, S. A. E. G. 2003, MNRAS, 344, 1210

Fatuzzo, M., & Adams, F.C. 2002, ApJ, 570. 210

Fiedler, R. A. & Mouschovias, T. Ch. 1992, ApJ, 391, 199

Fiedler, R. A. & Mouschovias, T. Ch. 1993, ApJ, 415, 680

Hawley, J. F., & Stone, J. M. 1995, Computer Physics Communications, 89, 127

Hayes, J. C., Norman, M. L., Fiedler, R. A., Bordner, J. O., Li, P. S., Clark, S. E., ud-Doula, A., & Mac Low, M.-M. 2005, ApJS, 165, 188

Hujeirat, A. & Rannacher, R. 2001, New Astr. Rev., 45, 425

Li, P. S., Norman, M. L., Mac Low, M.-M., & Heitsch, F. 2004, ApJ, 605, 818

Lintott, C. J., & Rawlings, J. M. C. 2006, A&A, 448, 425

Mac Low, M.-M., Norman, M. L., Konigl A., & Wardle, M. 1995, ApJ, 442, 726

Mac Low, M.-M. & Smith, M. D. 1997, ApJ, 491, 596

McKee, C.F. 1989, ApJ, 345, 782

Mestel, L. 1985, in *Protostars and Planets II*, ed. D. Black and M. Matthews (Tucson: University of Arizona Press), 320

Mestel, L., & Spitzer, L. 1956, MNRAS, 116, 503

Mouschovias, T. Ch. 1976a, ApJ, 206, 753

Mouschovias, T. Ch. 1976b, ApJ, 207, 141

Mouschovias, T. Ch. 1987, in *Physical Processes in Interstellar Clouds*, ed. G. Morfill & M. Scholer (Dordrecht: Reidel), 453

Norman, M. L. 2000, Rev. Mexicana Astron. Astrofis. Ser. Conf., 9, 66

Oishi, J. S. & Mac Low, M.-M. 2005, astro-ph/0510366

O′Sullivan, S. & Downes, T. P. 2005, astro-ph/0511478

Padoan, P., Zweibel, E., & Nordlund, Å. 2000, ApJ. 540, 332

Shu, F. H. 1983, ApJ, 273, 202

Shu, F. H. 1992, The Physics of Astrophysics, vol. II: Gas Dynamics (University Science Books)

Shu, F. H., Adams, F. C., & Lizano, S. 1987, ARA&A, 25, 23

Smith, M. D. & Mac Low, M.-M. 1997, A&A, 326, 801

Spitzer, L. 1942, ApJ, 95, 329

Tóth, G. 1995, MNRAS, 274, 1002

Wardle, M. 1990, MNRAS, 246, 98

Zweibel, E.G. 2002, ApJ, 567, 962

Zweibel, E.G., & Brandenburg, A. 1997, ApJ, 478, 563

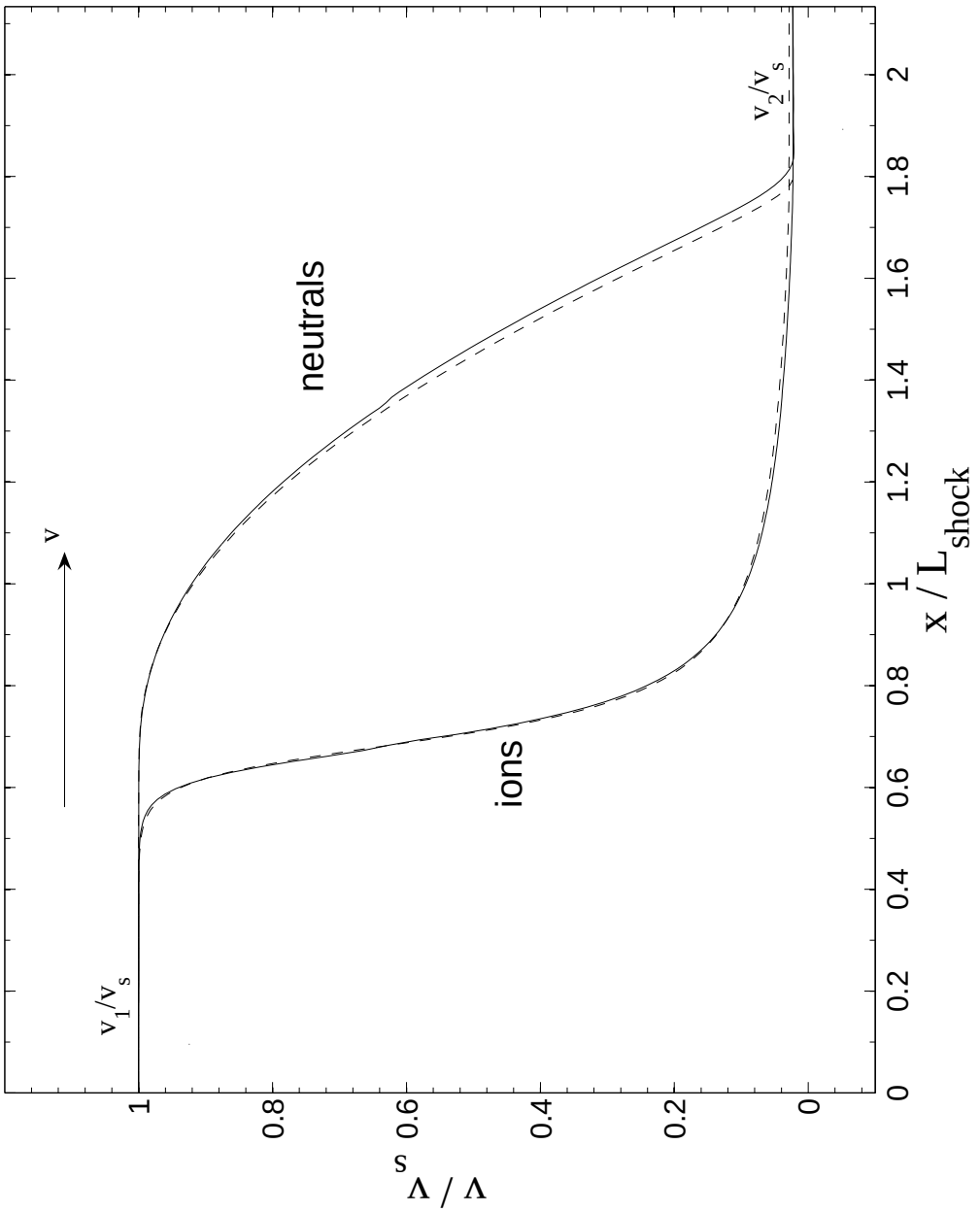

Fig. 1.— Velocities of the ions and neutrals in the C-type shock test. The flow is from left to right. The solid lines are the calculated results from ZEUS-MPAD; dashed curves are from analytic solutions (Smith & Mac Low 1997). Velocities are normalized by the shock velocity v_s and distance is normalized by the shock length.

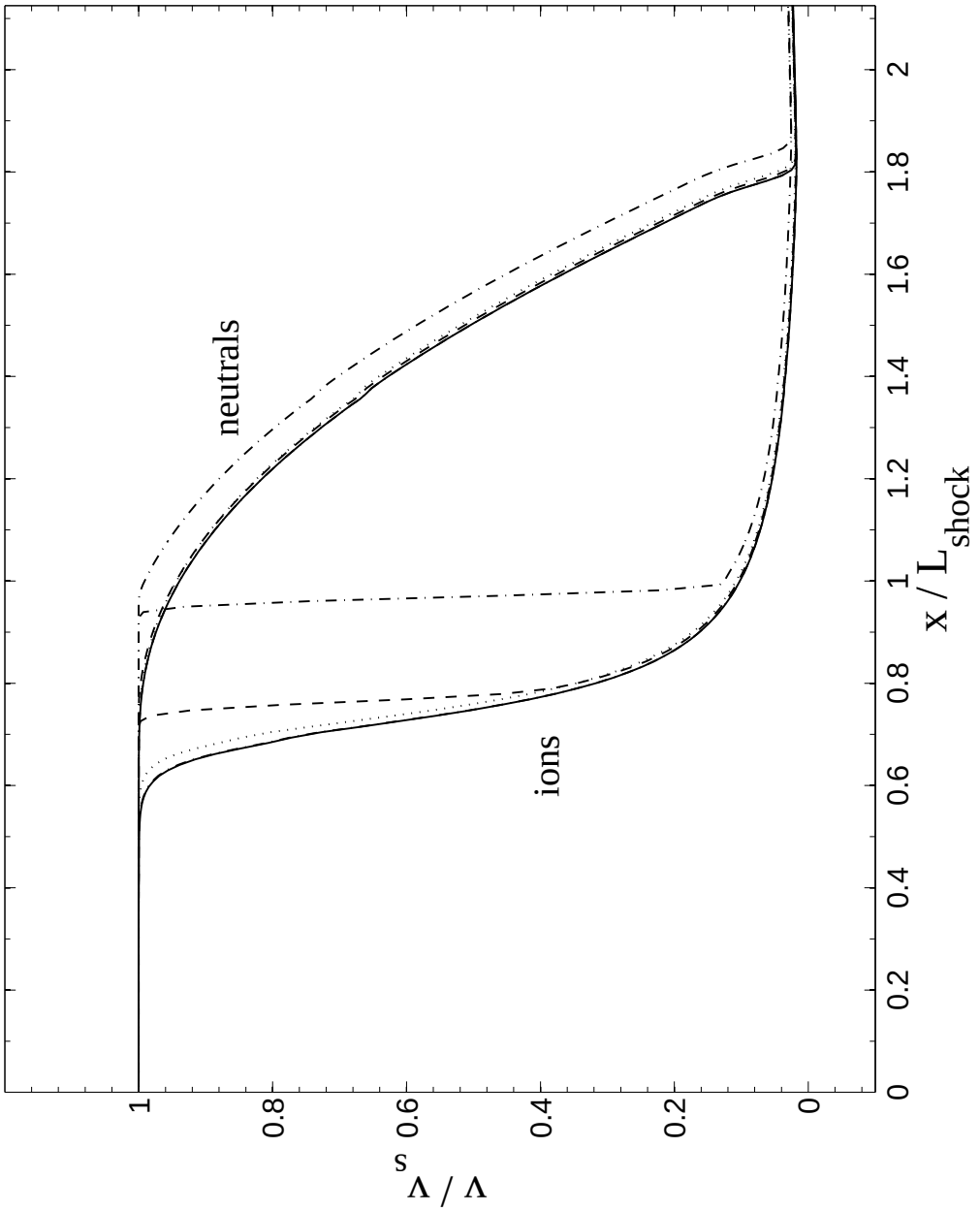

Fig. 2.— Velocities of the ions and neutrals in a C-type shock with different ion density ratios: $\mathcal{R} = 1$ ($\mathcal{M}_{Ai} = 0.052$, solid), 10 ($\mathcal{M}_{Ai} = 0.164$, dot-dot-dashed), 10^2 ($\mathcal{M}_{Ai} = 0.518$, dotted), 10^3 ($\mathcal{M}_{Ai} = 1.64$, dashed), 10^4 ($\mathcal{M}_{Ai} = 5.18$, dot dashed). The curves for $\mathcal{R} = 1$ and 10 are virtually indistinguishable. When $\mathcal{R} = 10^4$, the error is obvious even in the velocity of the neutrals.

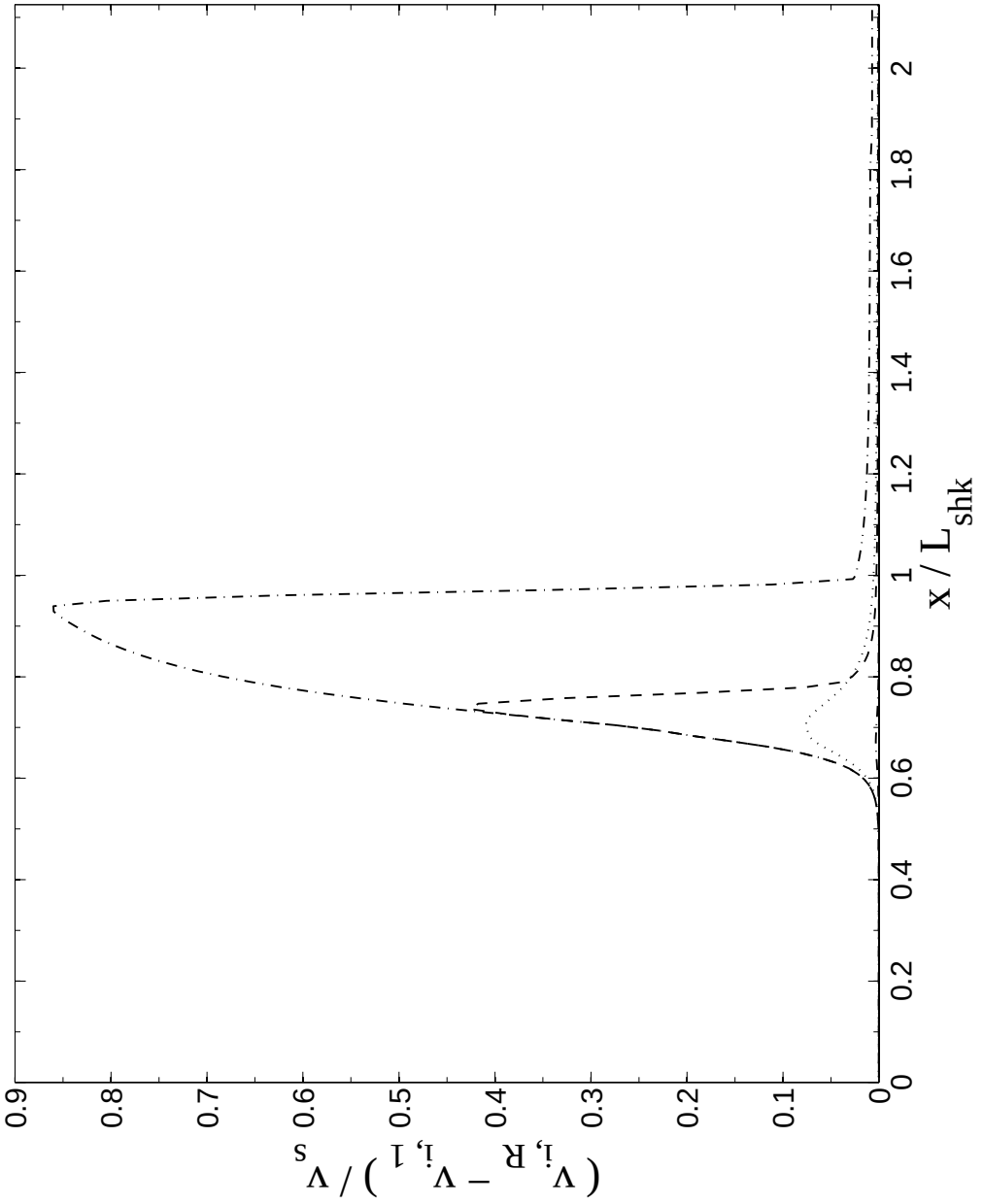

Fig. 3.— Normalized velocity differences of the ion component in the C-type shock tests corresponding to different ion density ratios: $\mathcal{R} = 10$ ($\mathcal{M}_{Ai} = 0.164$, solid), 10^2 ($\mathcal{M}_{Ai} = 0.518$, dotted), 10^3 ($\mathcal{M}_{Ai} = 1.64$, dashed), 10^4 ($\mathcal{M}_{Ai} = 5.18$, dot dashed). The ion velocity profile at $\mathcal{R} = 1$ is used as the reference.

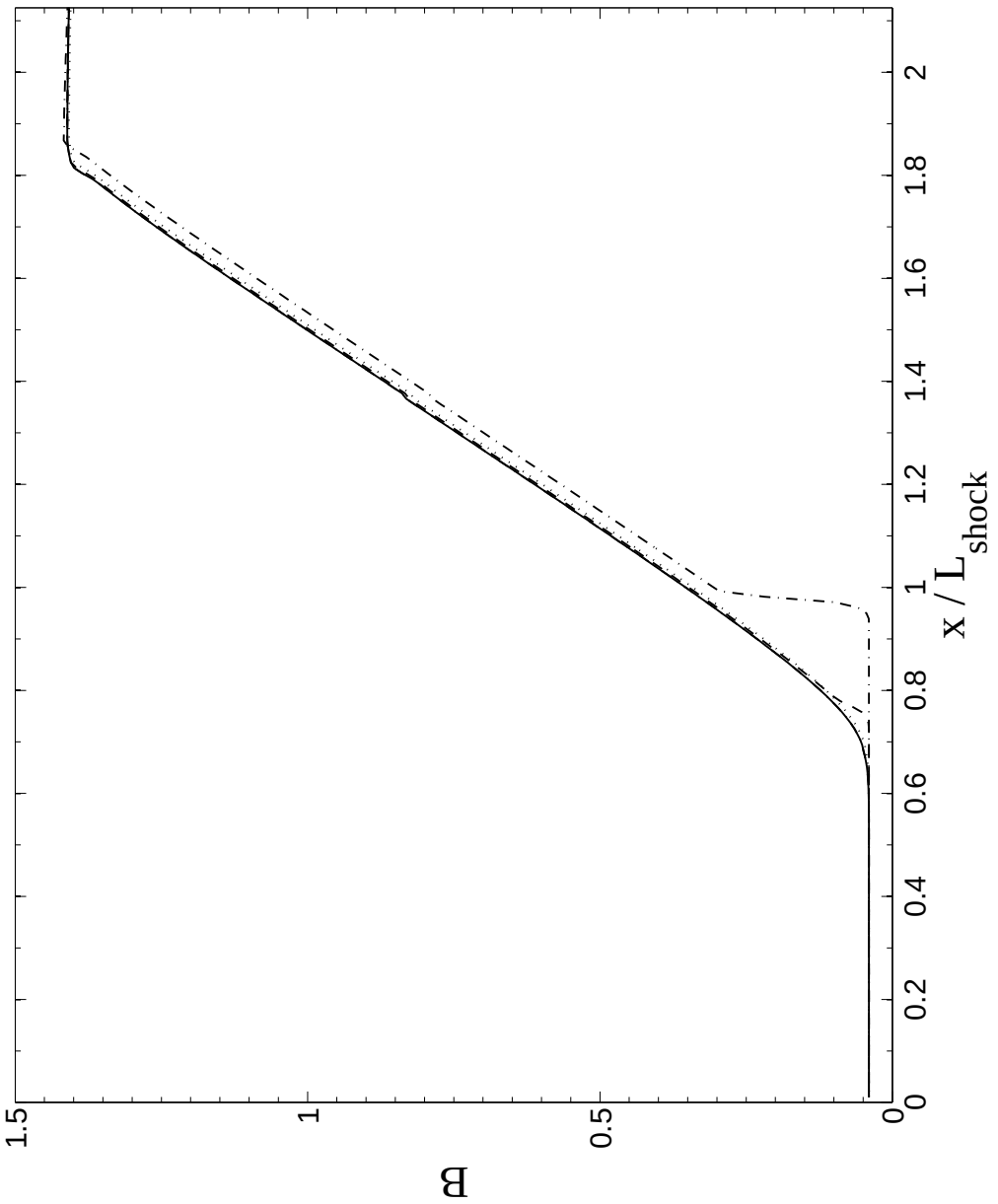

Fig. 4.— Scaled magnetic fields in the C-type shock tests with different ionization fractions: $\mathcal{R}$ = 1 ($\mathcal{M}_{Ai}$ = 0.052, solid), 10 ($\mathcal{M}_{Ai}$ = 0.164, dot-dot-dashed), 10^2 ($\mathcal{M}_{Ai}$ = 0.518, dotted), 10^3 ($\mathcal{M}_{Ai}$ = 1.64, dashed), 10^4 ($\mathcal{M}_{Ai}$ = 5.18, dot dashed). The curves for $\mathcal{R}$ = 1 and 10 are virtually indistinguishable. $\mathcal{R} = 10^4$, a large error occurs in the magnetic field near leading edge of the shock.

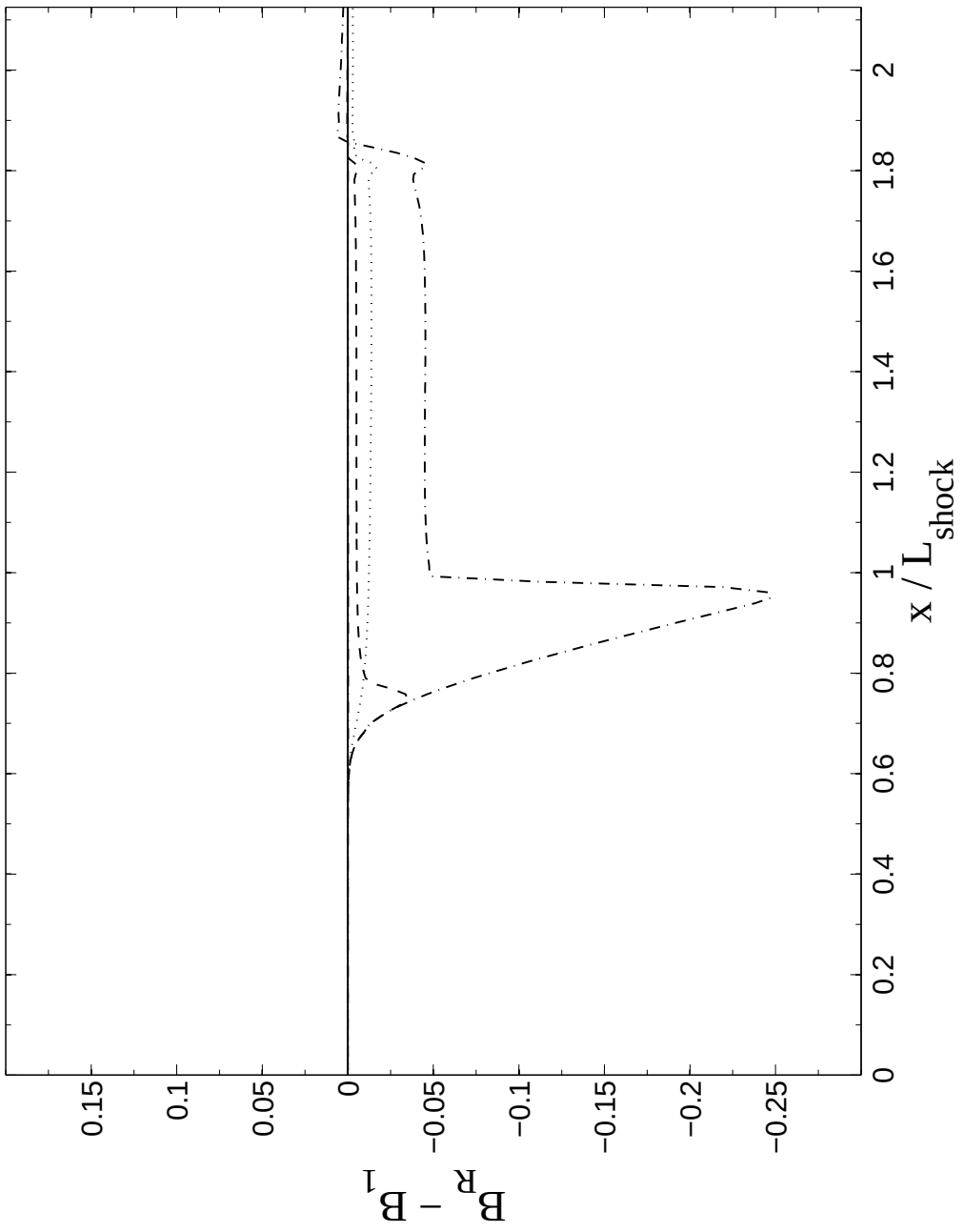

Fig. 5.— Scaled magnetic field differences in the C-type shock tests corresponding to different ionization fractions: $\mathcal{R} = 10$ ($\mathcal{M}_{Ai} = 0.164$, solid), 10^2 ($\mathcal{M}_{Ai} = 0.518$, dotted), 10^3 ($\mathcal{M}_{Ai} = 1.64$, dashed), 10^4 ($\mathcal{M}_{Ai} = 5.18$, dot dashed). The magnetic field profile at $\mathcal{R} = 1$ is used as a reference.

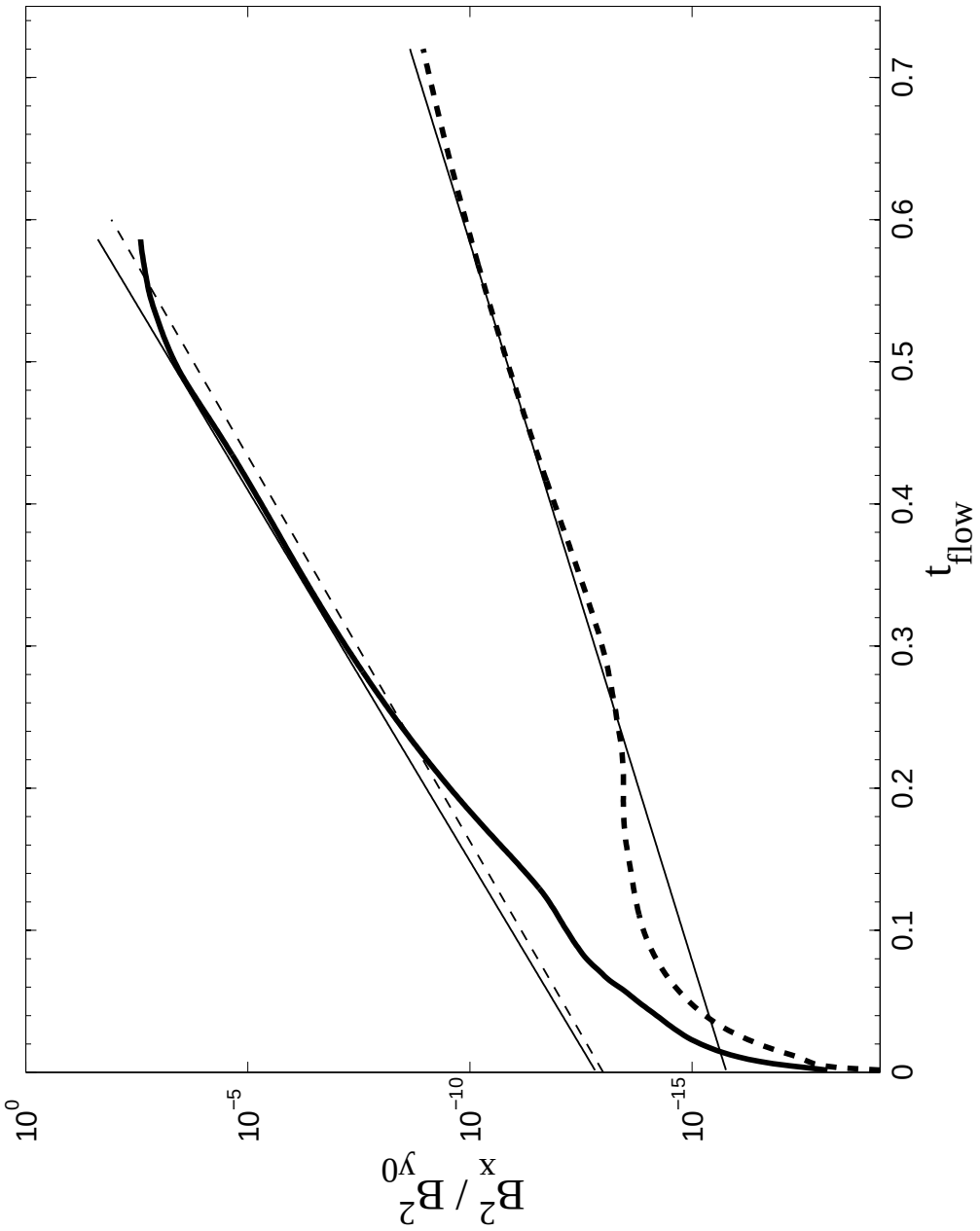

Fig. 6.— Wardle instability growth in 3D C-type shock tests. The instability growth rate is determined from the growth of magnetic energy in the direction parallel to the shock velocity. In the figure, this energy is normalized to the initial magnetic energy in the direction perpendicular to the shock velocity, B_x^2/B_y^2. The thick solid curve shows the growth of B_x^2/B_y^2 in the simulation with $\mathcal{R} = 10^2$ ($\mathcal{M}_{Ai} \sim 0.5$). The thick dashed curve shows the growth of B_x^2/B_y^2 in the simulation with $\mathcal{R} = 10^4$ ($\mathcal{M}_{Ai} \sim 5$). The two thin straight lines are the best fit for the exponential growth of the instability. The thin dashed line shows the expected growth rate from the analytic solution.

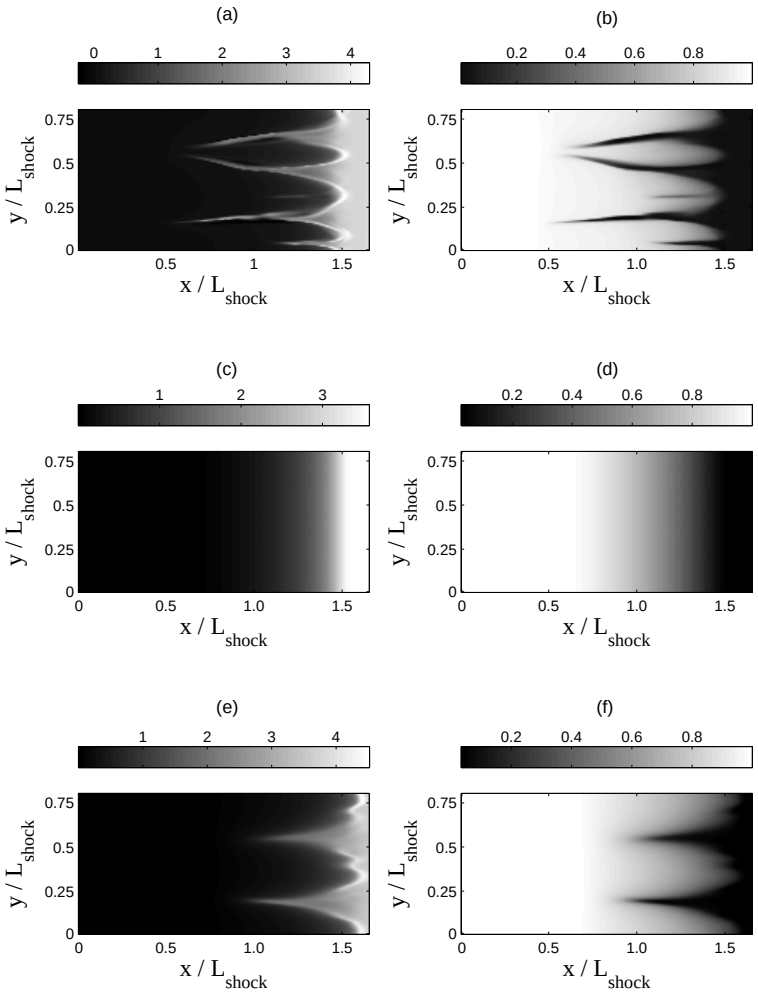

Fig. 7.— Velocities and logarithmic density slices of the neutral component in the two Wardle instability tests. (a) Logarithmic density slice with $\mathcal{R} = 10^2$ at $t = 0.54t_{ni}$ normalized by the initial upstream neutral density. (b) Velocity slice with $\mathcal{R} = 10^2$ at $t = 0.54t_{ni}$ normalized by the shock velocity. Spikes in the magnetic field are clearly seen at this time. (c) Logarithmic density slice with $\mathcal{R} = 10^4$ at $t = 0.54t_{ni}$ normalized by the initial upstream neutrals density. (d) Velocity slice with $\mathcal{R} = 10^4$ at $t = 0.54t_{ni}$ normalized by the shock velocity. The amplitude of the instability is small at this time. (e) Logarithmic density slice with $\mathcal{R} = 10^4$ at $t = 1.08t_{ni}$ normalized by the initial upstream neutrals density. (f) Velocity slice with $\mathcal{R} = 10^4$ at $t = 0.54t_{ni}$ normalized by the shock velocity. Instability occurs at a much later time when the ions are super-Alfvénic.

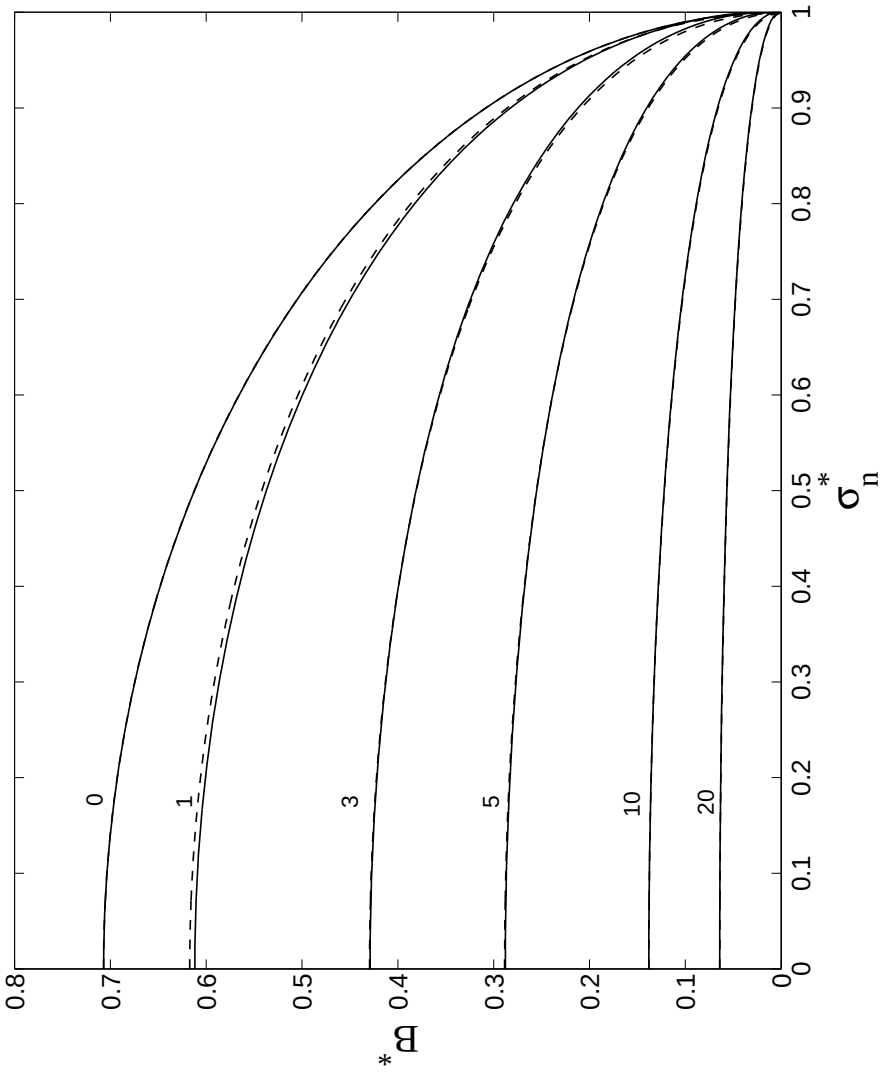

Fig. 8.— Time evolution of the dimensionless magnetic field, B^*, verses the normalized surface density, σ_n^*. The solid curves are results of model $\mathcal{R} = 33.3$ using ZEUS-MPAD. The dashed curves are results from integrating equations (44), (50), and (56) (see text). The normalized time, τ, is shown near each curve in the plot.

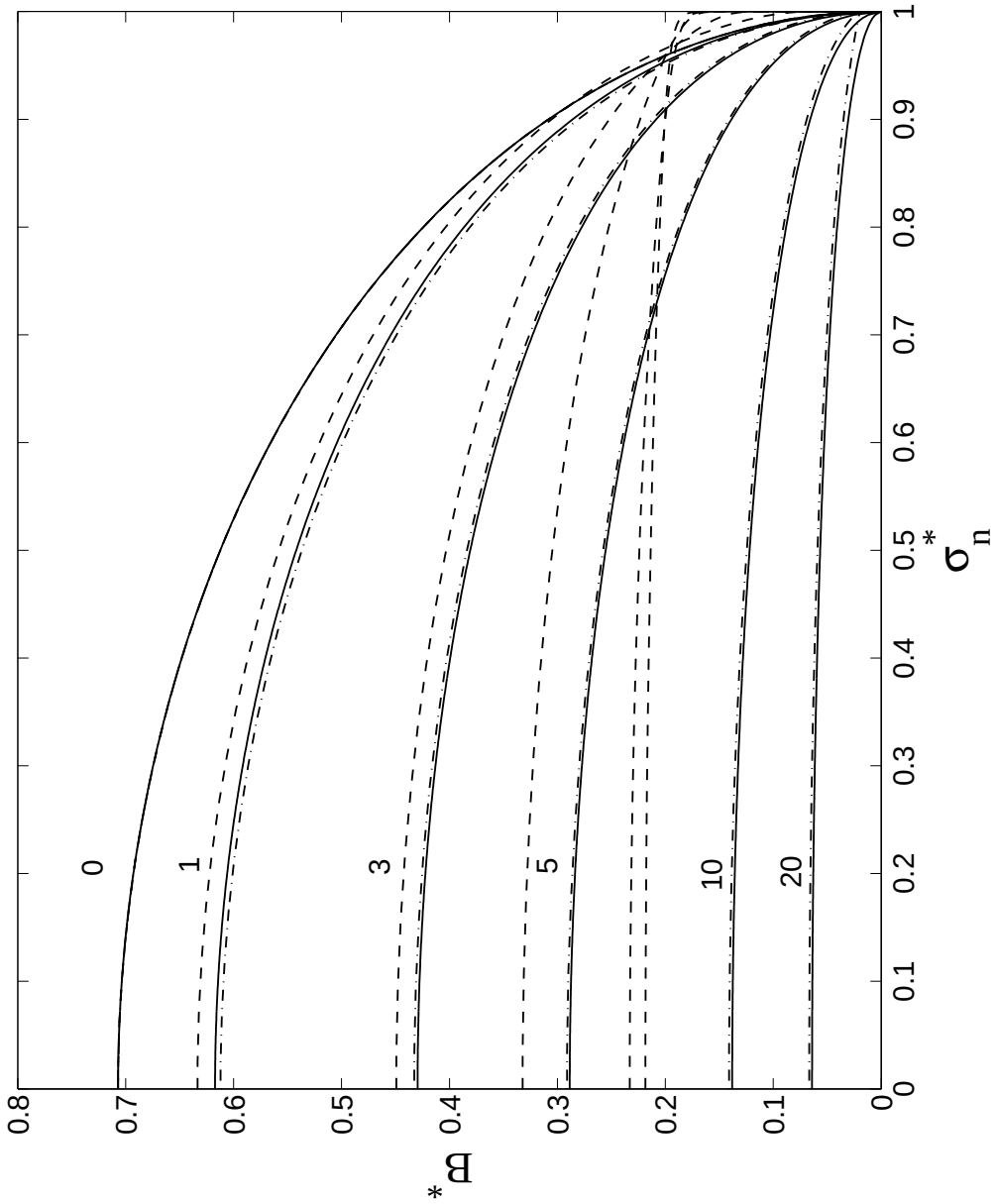

Fig. 9.— Time evolution of the dimensionless magnetic field, B^*, vs. the normalized neutral surface density, σ_n^*. The solid curves are results from integrating equations (44), (50), and (56). The ZEUS-MPAD $\mathcal{R} = 3.33 \times 10^4$ model (dashed) and $\mathcal{R} = 3.33 \times 10^2$ model results (dot-dashed) are also shown for comparison. Large deviations from the low-ionization results are seen in B^* when the ion mass ratio is large (see §3.3).

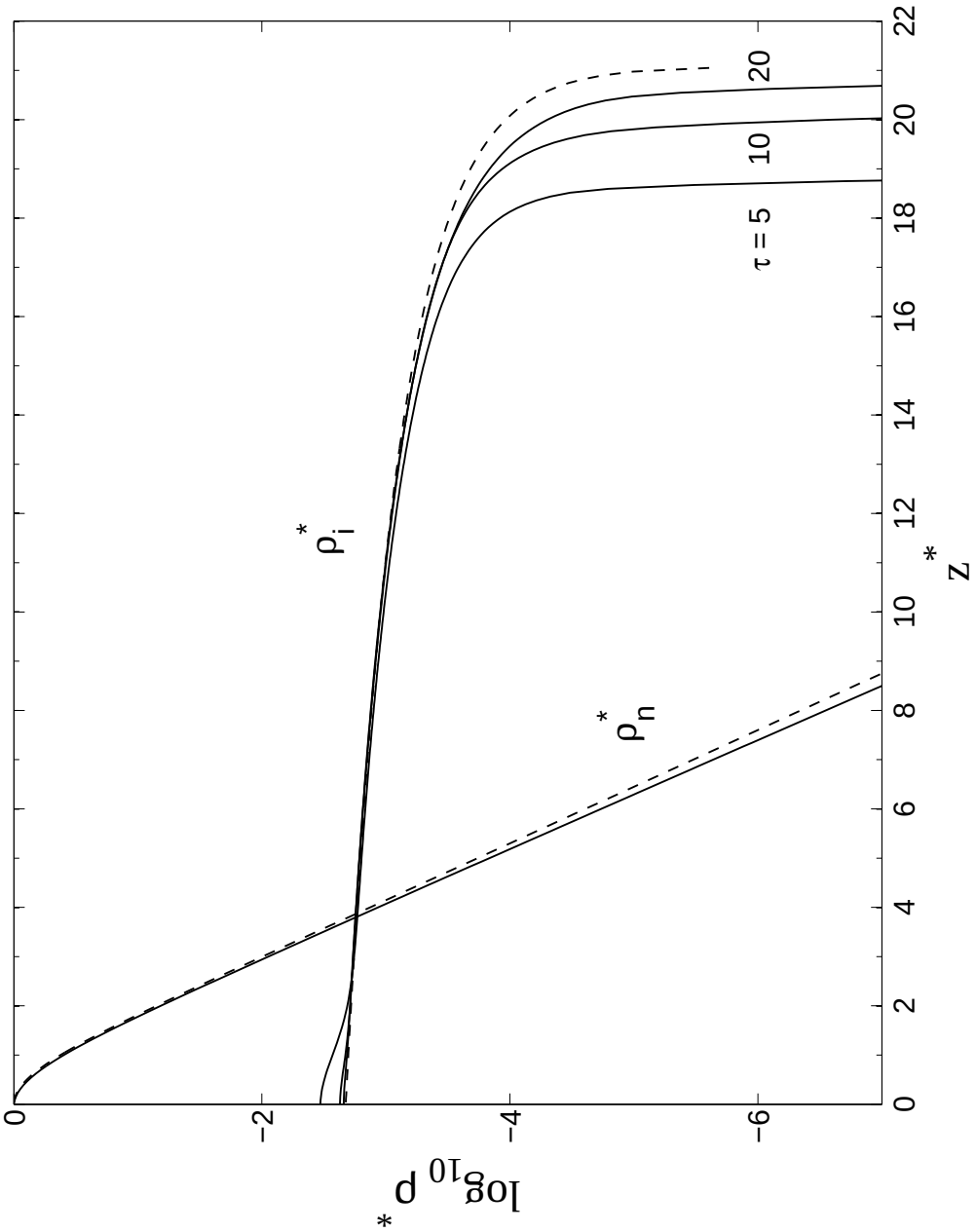

Fig. 10.— The dimensionless densities of neutrals ρ_n^* and ions ρ_i^* at $\tau = 5$, 10, and 20 from the ZEUS-MPAD $\mathcal{R} = 3.33 \times 10^4$ model (solid curves). The final state distributions predicted by equations (A2) and (A11) are shown for comparison (dashed curves).

Table 1: Percentage errors of ion velocity and magnetic field strength in C-type shock test for different ion Alfvén Mach numbers.

$\mathcal{R}$	$\mathcal{M}_{Ai}$	Err(v) %	Err (|B|) %
10^4	5.18	47.76	8.64
10^3	1.64	9.19	0.91
10^2	0.518	0.83	0.04
10^1	0.164	0.14	0.01